Nanoscale

PAPER

View Article Online
View Journal | View Issue

Cite this: *Nanoscale*, 2019, **11**, 9023

Fusion-dependent formation of lipid nanoparticles containing macromolecular payloads†

Jayesh A. Kulkarni, *‡[a,b] Dominik Witzigmann, ‡[a] Jerry Leung,[a] Roy van der Meel, [a,c,d] Josh Zaifman,[a,e] Maria M. Darjuan,[a,e] Hiu Man Grisch-Chan,[f] Beat Thöny, [f] Yuen Yi C. Tam[a,e] and Pieter R. Cullis *§[a]

The success of Onpattro™ (patisiran) clearly demonstrates the utility of lipid nanoparticle (LNP) systems for enabling gene therapies. These systems are composed of ionizable cationic lipids, phospholipid, cholesterol, and polyethylene glycol (PEG)-lipids, and are produced through rapid-mixing of an ethanolic-lipid solution with an acidic aqueous solution followed by dialysis into neutralizing buffer. A detailed understanding of the mechanism of LNP formation is crucial to improving LNP design. Here we use cryogenic transmission electron microscopy and fluorescence techniques to further demonstrate that LNP are formed through the fusion of precursor, pH-sensitive liposomes into large electron-dense core structures as the pH is neutralized. Next, we show that the fusion process is limited by the accumulation of PEG-lipid on the emerging particle. Finally, we show that the fusion-dependent mechanism of formation also applies to LNP containing macromolecular payloads including mRNA, DNA vectors, and gold nanoparticles.

Received 6th March 2019,
Accepted 20th April 2019

DOI: 10.1039/c9nr02004g

rsc.li/nanoscale

Introduction

Onpattro™ (patisiran) is the first RNA interference therapeutic approved by the FDA and EMA.[1,2] The technology enabling the delivery of therapeutic short interfering RNA (siRNA) is based on lipid nanoparticles (LNP). These systems are composed of ionizable cationic lipids (*e.g.* 2,2-dilinoleyl-4-(2-dimethylaminoethyl)-[1,3]-dioxolane (KC2)[3] or heptatriaconta-6,9,28,31-tetraen-19-yl-4-(dimethylamino)butanoate (MC3)[4]), phospholipid, cholesterol and polyethylene glycol-lipid.[5,6] LNP are generated through rapid-mixing techniques[7] where an ethanolic lipid solution is diluted into an acidic aqueous phase containing the anionic macromolecules. We have previously shown that LNP prepared in this way display high entrapment efficiencies (>85%) for anionic macromolecules such as siRNA[8] and plasmid DNA (pDNA),[9,10] or colloidal gold nanoparticles (GNP).[10]

LNP–siRNA systems display an electron-dense core as observed by cryogenic transmission electron microscopy (cryo-TEM).[11,12] It was originally suggested that this electron-dense core reflects inverted micellar structures generated by the association of ionizable cationic lipid with the anionic payload.[12] These hydrophobic structures were hypothesized to aggregate and then become coated with a monolayer of polar lipids such as PEG-lipids as these lipids reach their solubility limits in the ethanol/water mixture. This hypothesis implied that the final LNP structure is established during (and as a result of) the rapid-mixing process.[5,6,8,12,13] Recently, we re-examined the LNP–siRNA structure, demonstrating that the LNP electron-dense core morphology does not consist of inverted micelles but reflects an oil core consisting primarily of neutral ionizable lipid,[11] and suggested that LNP–siRNA formulations are generated through fusion of smaller particles that occurs after the rapid-mixing procedure. While much of that work was performed with the ionizable lipid KC2, the same structures and mechanism of formation are seen for LNP with the Onpattro™ composition (containing MC3; ESI Fig. S1†).

[a]*Department of Biochemistry and Molecular Biology, University of British Columbia, 2350 Health Sciences Mall, Vancouver, British Columbia, Canada V6T 1Z3. E-mail: pieterc@mail.ubc.ca, j.kulkarni@alumni.ubc.ca; Fax: +1 (604)-822-4843; Tel: +1 (604)-822-4144*

[b]*Department of Medical Genetics, University of British Columbia, 950 West 28th Avenue, Vancouver, British Columbia, V5Z 4H4, Canada*

[c]*Department of Clinical Chemistry and Haematology, University Medical Center Utrecht, Utrecht, The Netherlands*

[d]*Laboratory of Chemical Biology, Department of Biomedical Engineering and Institute for Complex Molecular Systems, Eindhoven University of Technology, Eindhoven, The Netherlands*

[e]*Integrated Nanotherapeutics, 6190 Agronomy Road, Vancouver, British Columbia, Canada V6T 1Z3*

[f]*Division of Metabolism, University Children's Hospital Zurich and Children's Research Centre, Steinwiesstrasse 75, 8032 Zurich, Switzerland*

†Electronic supplementary information (ESI) available. See DOI: 10.1039/c9nr02004g

‡Contributed equally.

§Present address: Life Sciences Institute, University of British Columbia, 2350 Health Sciences Mall, Vancouver, British Columbia, Canada V6T 1Z3.

In this work, we further elucidate the mechanism of LNP formation following the rapid-mixing step for LNP systems using an electron microscopy- and fluorescence-based approach. We examine the role of PEG-lipids in limiting the fusion process and extend our investigation of LNP morphology to include larger payloads such as messenger RNA (mRNA), minicircle DNA (mcDNA), pDNA, or GNP. Results obtained support the proposal that LNP formation occurs through a pH-dependent fusion process that occurs subsequent to the rapid mixing event, and that the formation of LNP with large payloads builds on formation of LNP formed at pH 4 that contain mRNA, mcDNA or pDNA.

Materials and methods

Materials

The lipids 1,2-distearoyl-*sn-glycero*-3-phosphorylcholine (DSPC) and 1,2-distearoyl-*sn-glycero*-3-phosphoethanolamine-*N*-[methoxy(polyethylene glycol)-2000] (ammonium salt) (PEG-DSPE) were purchased from Avanti Polar Lipids (Alabaster, AL). The ionizable amino-lipid 2,2-dilinoleyl-4-(2-dimethylaminoethyl)-[1,3]-dioxolane (KC2) was synthesized by Biofine International (Vancouver, BC). Cholesterol was purchased from Sigma-Aldrich (St Louis, MO). Heptatriaconta-6,9,28,31-tetraen-19-yl 4-(dimethylamino)butanoate (MC3)[4] and (*R*)-2,3-bis(tetradecyloxy)propyl-1-(methoxy polyethylene glycol 2000) carbamate (PEG-DMG)[14] were synthesized as previously described. Lipophilic indocarbocyanine dyes 3,3′-dioctadecyloxacarbocyanine perchlorate (DiO) and 1,1′-dioctadecyl-3,3,3′,3′-tetramethylindocarbocyanine perchlorate (DiI) were purchased from ThermoFisher Scientific (Waltham, MA). TEM grids and gold nanoparticles were purchased from Ted Pella, Inc. (Redding, CA). mRNA encoding firefly luciferase was purchased from TriLink Biotechnologies (San Diego, CA). pDNA encoding TdTomato[15] was purchased from Addgene (Cambridge, MA) and prepared using a Qiagen Endotoxin-free Giga prep kit (Hilden, Germany). Minicircle DNA (mcDNA) was generated by transforming the mcDNA producer plasmids into *E. coli* ZYCY10P3S2T and purification of resulting mcDNA vectors using the Qiagen Endotoxin-free plasmid purification kit as previously described.[16] siRNA against firefly luciferase[17] was purchased from IDT (Coralville, IA).

Preparation of empty LNP

LNP were prepared as previously described.[9,11] Briefly, lipid components (KC2, Chol, DSPC, and PEG-lipid) at appropriate ratios were dissolved in ethanol to a concentration of 10–15 mM total lipid. *For fluorescence resonance energy transfer (FRET) experiments*: non-exchangeable donor or acceptor lipid tracers (DiO or DiI, respectively) were added to lipid mixtures at a concentration of 0.2 mol%.

The aqueous phase consisted of 25 mM sodium acetate pH 4 buffer. The two solutions were mixed through a T-junction mixer[18,19] at a total flow rate of 20 mL min^{-1}, and a flow rate ratio of 3 : 1 v/v (corresponding to 15 : 5 mL min^{-1} aqueous : organic phase). Unless otherwise specified, the resulting suspension was subsequently dialysed against 1000-fold volume of the same sodium acetate pH 4 buffer or against phosphate buffered saline (PBS pH 7.4).

For post-formation PEG-insertion studies: LNPs were prepared with KC2, DSPC and Chol (no PEG-lipid) using the rapid-mixing technique described above, where the ethanolic lipid phase was combined with a 25 mM sodium acetate pH 4 buffer. Following dialysis into the same pH 4 buffer to remove ethanol the resulting LNPs were concentrated to achieve a final concentration of 2.5 mM total lipid. PEG-lipid dissolved in ethanol was added to appropriate amounts to achieve 0.5–2.5 mol% PEG-lipid. At all molar fractions of PEG, the total amount of ethanol in the mixture was 1% v/v. The solutions were pipette-mixed and the resulting mixture was dialysed against 1000-fold volume of PBS overnight.

FRET-based fusion assay

LNP–DiO, LNP–DiI or LNP–DiO/LNP–DiI mixtures (equimolar concentrations) at pH 4 or pH 7.4 were diluted using sodium acetate pH 4 buffer or PBS pH 7.4. Samples were excited at 470 nm and the emission was collected between 505–650 nm. FRET data from each set of experiment were normalized to emission of donor probe (LNP–DiO) under identical conditions. Spectroscopic evidence for FRET could be observed by decrease of fluorescence at 505 nm and increase at 570 nm.

Preparation of LNP containing nucleic acid

LNP–nucleic acid were prepared as previously described.[9,11] Briefly, lipid components (KC2, Chol, DSPC, and PEG-lipid) at appropriate ratios were dissolved in ethanol to a concentration of 10–15 mM total lipid. Purified nucleic acid polymers were dissolved in 25 mM sodium acetate pH 4 buffer to achieve a ratio of 0.029 mg nucleic acid per μmol lipid (corresponding to amine-to-phosphate (N/P) ratio of 6) unless otherwise specified. The two solutions were mixed through a T-junction mixer[18,19] at a total flow rate of 20 mL min^{-1}, and a flow rate ratio of 3 : 1 v/v (corresponding to 15 : 5 mL min^{-1} aqueous : organic phase). The resulting suspension was subsequently dialysed against the same sodium acetate pH 4 buffer or directly against PBS pH 7.4.

Preparation of LNP containing gold nanoparticles (GNP)

LNP–GNP were prepared using a modified process from that described elsewhere.[10] Briefly, lipid components (KC2, Chol, DSPC, and PEG-lipid) at appropriate ratios were dissolved in ethanol to a concentration of 10–15 mM total lipid. 5 nm GNP with a tannic-acid surface modification (Ted Pella, Redding, CA) were suspended in 25 mM sodium acetate pH 4 to a concentration of 2.2×10^{13} GNP μmol^{-1} lipid. In order to maintain the same charge ratio (negative charges of the GNP to positively charged lipid), 12 nm GNP were formulated at 3.82×10^{12} GNP μmol^{-1} lipid. This number was generated based on maintaining a constant ratio of surface area of GNP to amount of lipid (1.73×10^{15} nm^2 μmol^{-1} lipid). The two solutions were mixed through a T-junction mixer[18,19] at a total flow rate of

20 mL min^{-1}, and a flow rate ratio of 3 : 1 v/v (corresponding to 15 : 5 mL min^{-1} aqueous : organic phase). The resulting suspension was subsequently dialysed against the same sodium acetate pH 4 buffer or directly against PBS pH 7.4. For studies including a mixture of 5 and 12 nm GNP, the LNP systems were always mixed after the rapid-mixing process.

Cryogenic transmission electron microscopy (cryo-TEM)

Cryo-TEM was performed as previously described.[11] LNP suspensions were concentrated to a final concentration of 20–25 mg mL^{-1} of total lipid and added to glow-discharged copper grids (3–5 μL), and plunge-frozen using a FEI Mark IV Vitrobot (FEI, Hillsboro, OR) to generate vitreous ice. Grids were stored in liquid nitrogen until imaged. Grids were moved into a Gatan 70° cryo-tilt transfer system pre-equilibrated to at least −180 °C prior to insertion into the microscope. An FEI LaB6 G2 TEM (FEI, Hillsboro, OR) operating at 200 kV under low-dose conditions was used to image all samples. A bottom-mount FEI Eagle 4 K CCD camera was used to capture all images. All samples (unless otherwise stated) were imaged at a 55 000× magnification with a nominal under-focus of 1–2 μm to enhance contrast. Sample preparation and imaging was performed at the UBC Bioimaging Facility (Vancouver, BC).

Analysis of LNPs

Cryo-TEM micrographs obtained for each sample were characterized for particle size (as compared by length to the scale bar), performed by manual counting of at least 150 LNPs to account for scattering interference from different morphology. Such an approach has been shown to closely correlate with the number-weighted average produced by dynamic light scattering.[20] Similarly, the fraction of loaded LNPs was performed manually. Lipid concentrations were measured using the Cholesterol E Total-Cholesterol assay (Wako Diagnostics, Richmond, VA). RNA entrapment was measured using the procedure described elsewhere.[21]

Statistical analysis

Statistical analyses were performed for all quantitative data using GraphPad. Where applicable, two-way ANOVAs were performed using the Tukey multiple comparison test and confidence level of 0.001. Similarly, where applicable an unpaired *t*-test was performed. All significance values are provided in the figure legends or in the ESI.†

Results and discussion

FRET and Cryo-TEM studies demonstrate fusion of precursor liposomes

Initial studies were focused on characterizing the fusion events following the rapid mixing of KC2/DSPC/Chol/PEG-lipid (50/10/39/1 mol%) in ethanol with an aqueous stream of 25 mM acetate buffer pH 4 buffer to form "empty" LNP systems. The resulting mixture was then dialyzed against the acetate buffer to remove ethanol, or against phosphate buffered saline (PBS) pH 7.4 to remove solvent and neutralize the pH. In agreement with previous studies,[11] the empty LNP display small bilayer structures at pH 4 where KC2 ($pK_a \sim 6.7$) is protonated but form larger electron-dense structures at pH 7.4 (Fig. 1A/B). In order to directly demonstrate that the larger structures result from fusion of structures formed at pH 4, LNP were formulated with non-exchangeable fluorescence resonance energy transfer (FRET) lipid tracers; either a donor probe (DiO; green; Ex 484 nm, Em 501 nm) or an acceptor probe (DiI; red; Ex 549 nm, Em 565 nm), which are able to act as a FRET pair when in close proximity,[22] *i.e.* present in the same LNP. If the particles fuse, a FRET signal would be expected as emission at 565 nm, when excited at 470 nm. As shown in Fig. 1C (top left), when the two formulations are combined at pH 4, the emission profile was an additive effect of two separate LNP formulations (no FRET). However, when LNP–DiO and LNP–DiI were combined at pH 4 and neutralized with addition of PBS, a clear FRET signal was observed (Fig. 1C, top right). In order to determine if lipid mixing occurred after the pH was raised to 7.4, LNP–DiO and LNP–DiI at pH 7.4 were combined and then the pH was lowered to 4 (Fig. 1C, bottom left) – no FRET signal was observed. Similarly, LNP combined at pH 7.4 and diluted with the same buffer did not display a FRET signal (Fig. 1C, bottom right). These data provide clear evidence that raising the pH from 4 to 7.4 promotes fusion of particles and that no lipid exchange occurs following this fusion process.

PEG-lipids limit fusion and dictate particle size

We next examined the role of PEG-lipids in determining the equilibrium size of these LNP. Previous work has shown that PEG-lipids reside primarily on the LNP surface where they exhibit a large area per molecule at the polar-non-polar interface of approximately 26 nm^2 (for PEG_{2000}).[8] As a result, the proportion of PEG-lipid dictates the size of the LNP as the concentration of PEG-lipid on the surface approaches a critical level that inhibits further fusion.[8,12,21] Here, we show that empty LNP composed of KC2/DSPC/Chol/PEG-lipid (50/10/37.5–39.5/0.5–2.5 mol%) form bilayer structures at pH 4 (Fig. 2A). Regardless of PEG-lipid content, the particle size at pH 4 is ~17 nm (Fig. 2B), but ranges from 31.9 nm (2.5 mol%) to 58.1 nm (0.5 mol%) at pH 7.4 (Fig. 2C), indicating that the PEG-lipid exerts its size-limiting role during neutralization of the pH. In order to demonstrate this more directly, LNPs composed of only KC2, DSPC and cholesterol (without PEG) were formulated by ethanol dilution/rapid mixing at pH 4 and dialyzed into the pH 4 buffer to remove solvent. PEG-lipid was then added into the LNP suspension from ethanol stocks, briefly mixed and the pH raised to pH 7.4 through dialysis. The resulting particle sizes were identical to particles where PEG-lipid is included in the initial ethanolic lipid phase (Fig. 2C).

Since the area per membrane lipid at the membrane–water interface is dependent on the size of the headgroup,[23] it would be expected that the area per molecule of the PEG-lipids will depend on the size of the PEG-moiety. LNPs were formulated

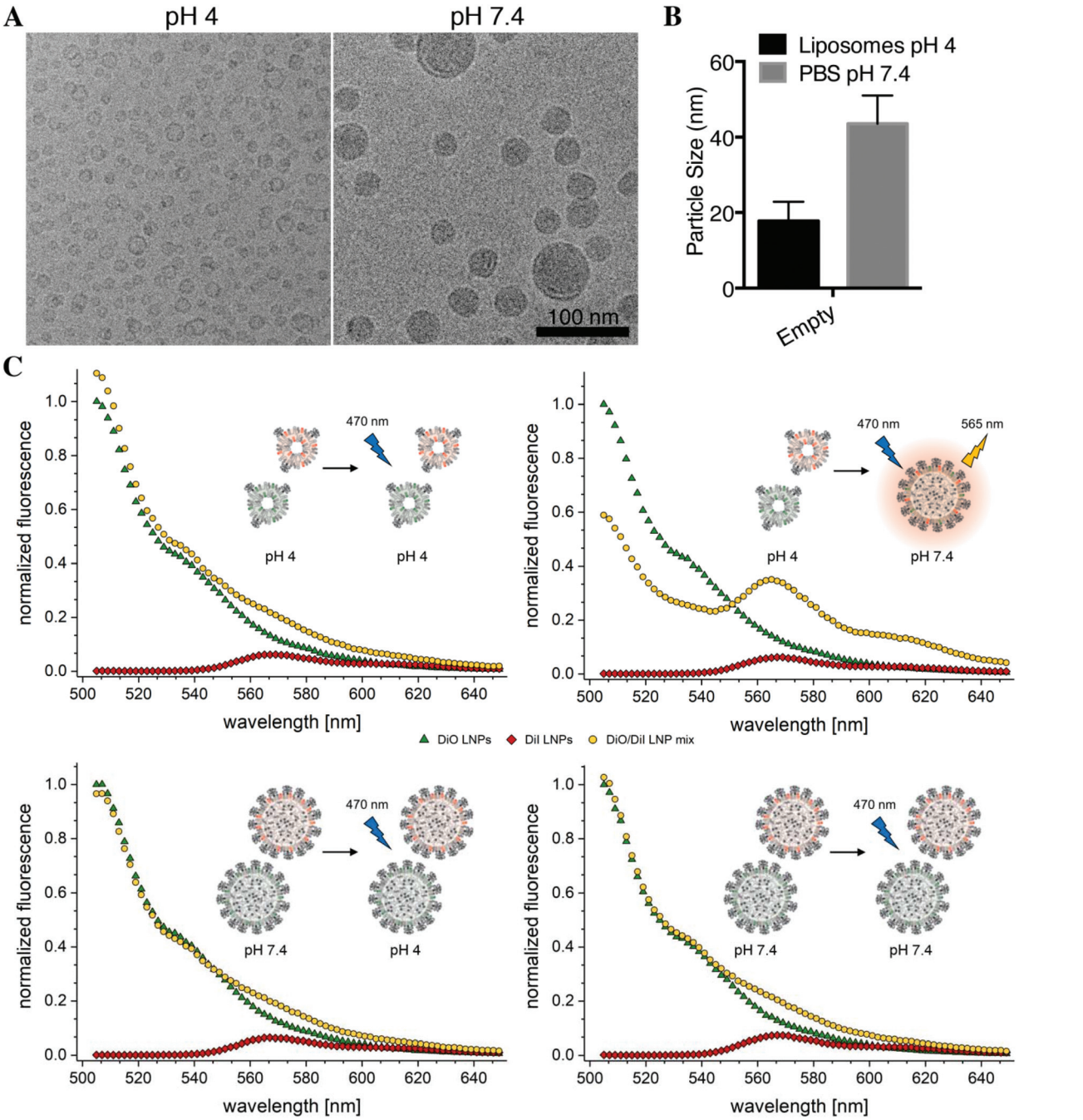

Fig. 1 Empty LNP observed as electron-dense structures are generated through fusion of smaller vesicular structures. (A) Empty LNP composed of KC2/Chol/DSPC/PEG-lipid (50/10/39/1 mol%) were generated at pH 4 and dialyzed into pH 4 buffer to remove solvent, or dialysed into PBS pH 7.4 to remove solvent and neutralize the pH. Scale bar = 100 nm. (B) Particle sizes of LNP at pH 4 and pH 7.4 as determined by manual measurement of 200 particles. Unpaired *t*-test, $p < 0.0001$. (C) LNP–DiO (donor) and LNP–DiI (acceptor) systems were combined under different conditions to determine if particle fusion generated a FRET signal. *Top left*: Formulations prepared in pH 4 were combined in pH 4 buffer. *Top right*: Formulations prepared in pH 4 buffer were combined and the pH was neutralized (pH 7.4). Note this is the only condition which resulted in FRET. *Bottom left*: Formulations prepared in PBS were combined in pH 4 buffer. *Bottom right*: Formulations prepared in PBS were combined and diluted in PBS. Each panel has an inset describing the experiment.

with PEG-lipid covering the PEG molecular weight range of 350–3000 g mol^{-1} (at molar fractions of 0.25–5 mol%). As shown in ESI Fig. 2,† decreasing the size of the PEG-chain results in significantly larger particles, and increasing the molar fraction of PEG-lipid results in smaller particles. Using the mathematical model described previously,[8] the corresponding area per PEG-lipid was determined to be 1.3–2 nm^2 for PEG_{350} (large size distributions), 6.5 nm^2 for PEG_{750}, 26 nm^2 for PEG_{2000} (as previously observed),[8] and 45 nm^2 for PEG_{3000}.

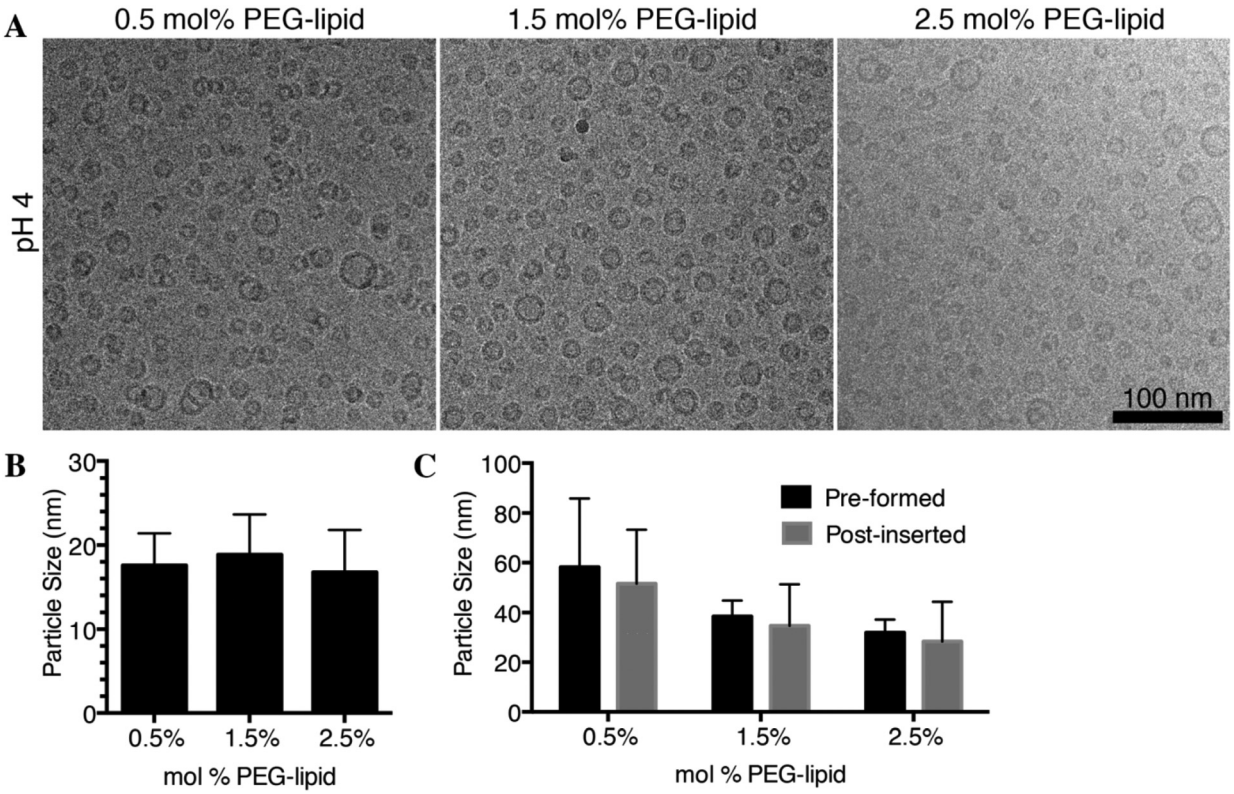

Fig. 2 PEG-lipid limits the number of particles that fuse to form the final LNP suspension at pH 7.4. (A) LNP composed of KC2/DSPC/Chol/PEG-lipid at molar ratios of 50/10/37.5–39.5/0.5–2.5 (respectively) were prepared in pH 4 buffer through rapid-mixing, and dialyzed into pH 4 buffer to remove solvent. Scale bar = 100 nm. (B) Particle sizes of LNP at pH 4 as determined by manual measurement of 200 particles. (C) Particle size of LNP prepared at pH 7.4 by addition of PEG-lipid at various stages of LNP formation. Formulations composed of KC2, DSPC, and Chol (with or without PEG-lipid) were generated using the rapid-mixing method. The *pre-formed* LNP mixture contained the appropriate amount of PEG-lipid in the ethanolic phase during rapid-mixing (black bars). For another set of formulations (termed *post-inserted*), particles were prepared without PEG-lipid and dialysed into pH 4 buffer to remove solvent. PEG-lipid was then added into the LNP suspension from ethanol stocks (total ethanol content was 1% v/v) and dialysed against PBS overnight (grey bars). The resulting particles were analysed by DLS. Results indicate number mean ± standard deviation.

LNP formulations of mRNA, mcDNA and pDNA are formed through fusion

It has been demonstrated previously that the ethanol-dilution rapid-mixing formulation process can also be applied to efficiently encapsulate large RNA and DNA payloads such as mRNA[10,24] and plasmid DNA.[9,10] It may be expected that the large size of these molecules will influence the size of the LNP formed at pH 4 that contain nucleic acid. LNP were formulated with mRNA (1.9 kb), mcDNA (1.4 and 3.4 kb-pairs) and plasmid DNA (5.6 kb-pairs) and characterized by cryo-TEM. It was found that LNP at pH 4 displayed two distinct populations: small liposomal structures and larger electron-dense particles (Fig. 3A). The electron-dense particles at pH 4 were marginally smaller than the electron-dense particles observed at pH 7.4 (Fig. 3B). The obvious difference between siRNA and pDNA is the size of the 21 bp duplex (42 negative charges) as compared to 5.6 kbp (11 200 negative charges). At an amine-to-phosphate (N/P) ratio of 1.5 (shown to be necessary to fully condense pDNA[25]), this corresponds to 1.68×10^4 ionizable cationic lipids per pDNA. Assuming a lipid density of 0.9 g mL^{-1}, this corresponds to a lipid volume of 3.66×10^4 nm^3 and a plasmid volume of 4.36×10^3 nm^3 per plasmid. The resultant LNP would be 42.8 nm in diameter if it contained one plasmid, and 52.7 nm if it contained two plasmids. The large electron-dense core structures (at pH 4) are 47.3 nm in diameter and likely contain one or two plasmids per particle. At pH 7.4, the average particle size increased to 59.4 nm. It is probable that the formulation is composed of a mixture of empty and pDNA-loaded LNP, however the cryo-TEM approach is unable to distinguish between these particles. It should be noted that for mRNA and mcDNA, the electron-dense structures (at pH 4) are larger than expected (calculated diameters for mRNA: 26.6 nm, mcDNA: 29.0 nm for 1.9 kbp and 36.7 nm for 3.4 kbp), this can be attributed to the presence of particles containing multiple mRNAs[26] or more than one mcDNA vector (*i.e.* multiple monomers or concatemers).[27]

GNPs shed light on the role and location of payload in LNP formation

The final set of studies concerned LNP systems containing GNP where the difference in density allows the negatively charged payload to be readily tracked using cryo-TEM. Here we first examined these structures at pH 4 and pH 7.4 by utilizing

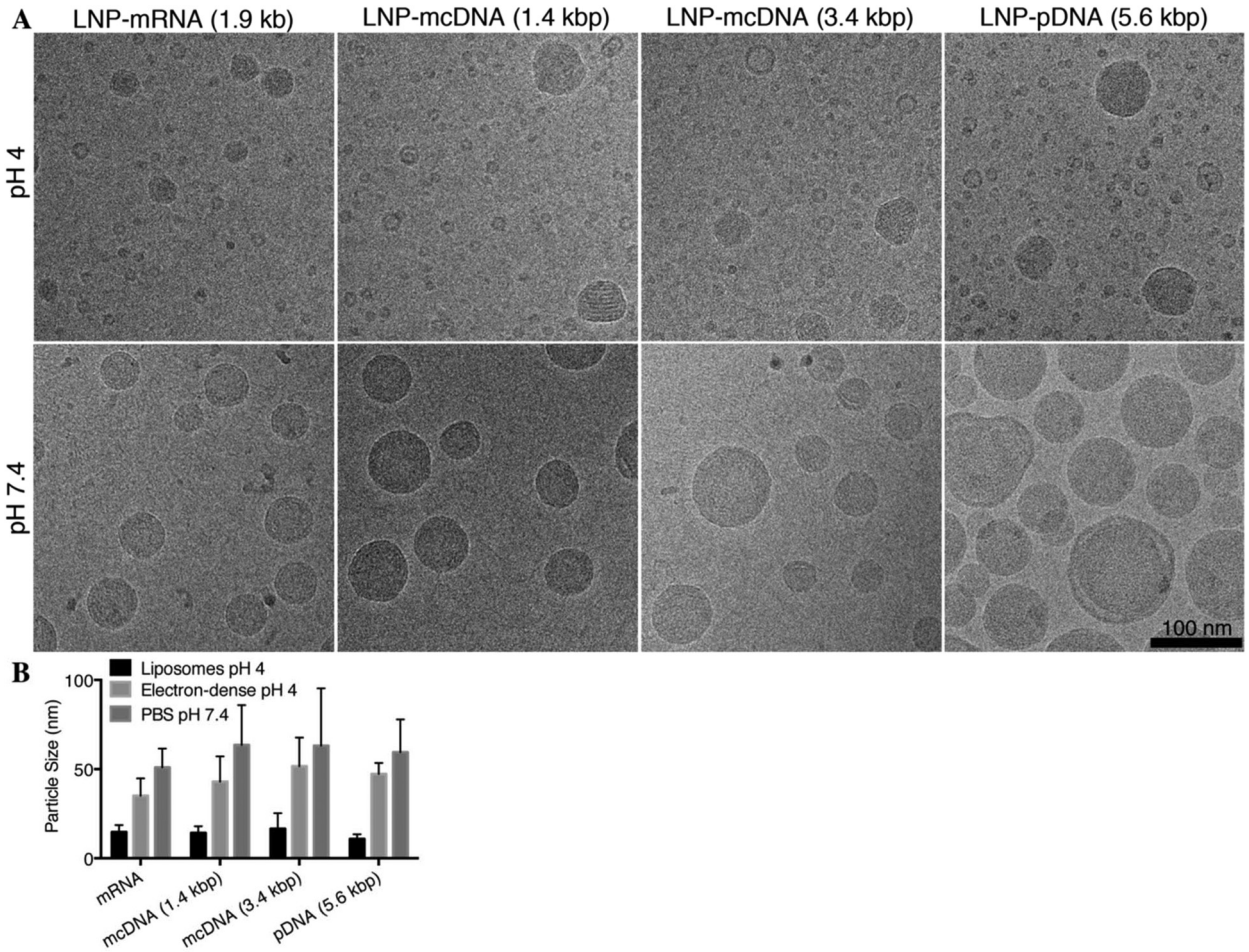

Fig. 3 LNP formations of various large nucleic acid polymers undergo fusion as the pH is neutralized to generate the final LNP system. (A) LNP composed of KC2/DSPC/Chol/PEG-lipid (50/10/39/1 mol%) as described elsewhere,[9,10] were prepared with nucleic acids (mRNA, mcDNA (1.4 and 3.4 kbp), and pDNA (5.6 kpb)) at pH 4 and dialyzed into pH 4 buffer to remove ethanol, or pH 7.4 buffer to remove ethanol and neutralize the pH. The resulting suspensions were concentrated and analyzed by cryo-TEM. Scale bar = 100 nm. (B) Particle sizing data of LNP systems at pH 4 divided into two categories: liposomes and electron-dense core structures, and particles at pH 7.4. In all cases n = 200, except for electron-dense core structures at pH 4, n = at least 40. 2-way ANOVA with Tukey's multiple comparisons correction was used to determine statistical difference. All LNP at pH 4 are identical in size $p > 0.5$. For detailed comparisons see ESI.†

5 nm GNP (Fig. 4A/B, respectively) and 12 nm GNP (Fig. 4C/D, respectively). The negative charge on GNPs results from the tannic-acid capping agent. Assuming a constant number of particles per volume, increasing the particle size would result in a different positive-to-negative charge ratio. To account for this, LNP–GNP formulations were generated at a GNP surface area-to-lipid ratio of 1.73×10^{15} nm^2 μmol^{-1} lipid. LNP systems clearly display evidence of bilayer structures at pH 4 (Fig. 4A/C), and much larger electron-dense particles at neutral pH (Fig. 4B/D). This indicates that the particles generated at pH 4 fully entrap the anionic payload during formation and the payload is located in structures that appear as electron-dense. Electron-dense particles at pH 4 are likely those that contain large nucleic acids (*i.e.* mRNA or DNA vectors), while other particles (*i.e.* small unilamellar vesicles) are payload-free.

It is of interest to determine whether LNP–GNP particles at pH 4 participated in the fusion process as the pH is raised or were "fully formed". LNP–GNP formulations were mixed at various stages of particle formation and imaged by cryo-TEM. First, LNP formulations of KC2/DSPC/Chol/PEG-lipid (50/10/39/1 mol%) containing both 5 and 12 nm GNP at pH 4 were combined and imaged (Fig. 4E). The resulting mixture displayed electron-dense particles containing either 5 or 12 nm GNPs, but no particles containing both GNP types. Next, LNP–GNP systems at pH 7.4 were combined (Fig. 4F). This mixture displayed electron-dense LNP containing either 5 or 12 nm GNPs suggesting no payload exchange between fully formed LNP. Third, when LNP–GNP formulations containing 5 nm GNP and 12 nm GNP were combined immediately after rapid-mixing at pH 4 and then dialyzed into PBS pH 7.4 to neutralize and remove solvent, LNP contained either 5 nm GNP, 12 nm GNP or a mixture of the two GNP sizes (Fig. 4G) indicating that the fusion process is not affected by the presence of encapsulated GNP. A similar experiment was performed combining LNP–GNP systems at pH 4 in the absence of solvent followed by neutralization using dialysis against PBS pH 7.4 (Fig. 4H).

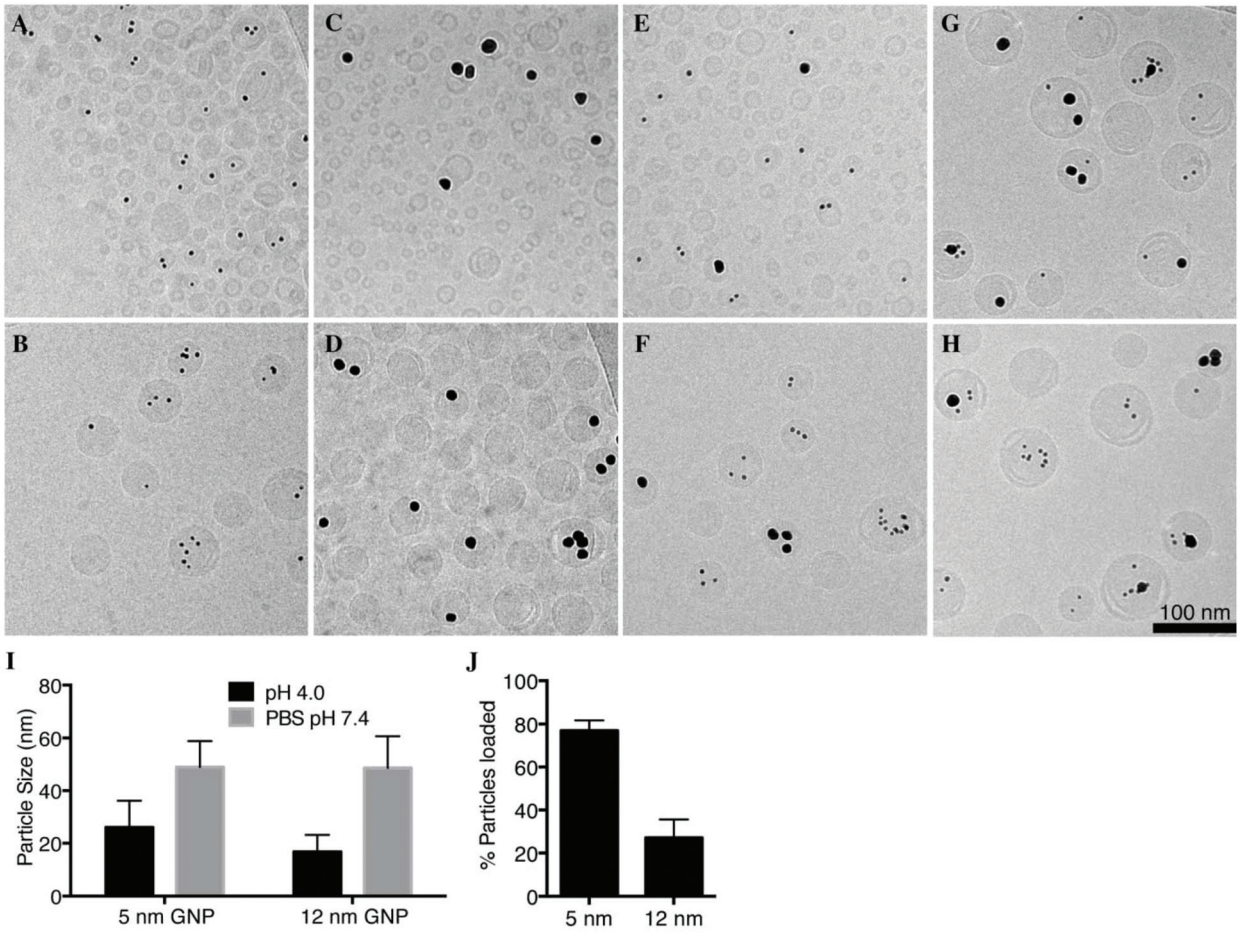

Fig. 4 LNP–GNP formulations containing either 5 or 12 nm GNP suggest particles with GNP at pH 4 participate in further fusion. LNP composed of KC2/DSPC/Chol/PEG-lipid (50/10/39/1 mol%) were prepared with 5 nm GNP (2.2×10^{13} GNP μmol^{-1} lipid) or 12 nm GNP (3.8×10^{12} GNP μmol^{-1} lipid) to maintain a constant GNP surface area of 1.73×10^{15} nm^2 μmol^{-1} lipid. LNP–$GNP_{5\ nm}$ were imaged by Cryo-TEM at pH 4 (A), and in PBS pH 7.4 (B). LNP–$GNP_{12\ nm}$ were imaged by Cryo-TEM at pH 4 (C), and at pH 7.4 (D). (E) The two formulations at pH 4 were combined and imaged. (F) Similarly, the formulations were prepared separately at pH 7.4 and then combined and imaged. (G) LNP–GNP systems were combined immediately following rapid-mixing (in the presence of 25% ethanol) and the pH raised to 7.4. (H) LNP–GNP at pH 4 were combined at pH 4 after dialysis to remove solvent, and the pH was neutralized. Scale bar = 100 nm. (I) Particle sizes of LNP at pH 4 and pH 7.4 as determined by manual measurement of 200 particles. 2-way ANOVA with Tukey's multiple comparisons correction was used to determine statistical difference. LNP–GNP at pH 7.4 are the same size. For detailed comparisons see ESI.† (J) Ten fields of Cryo-TEM images were analysed to determine the number of particles at pH 7.4 that are associated with GNP. The total number of particles counted were 220 per formulation and the percentage of loaded particles was determined.

As in Fig. 4G, LNP contained either 5 nm GNP, 12 nm GNP or a mixture of both 5 and 12 nm GNPs. As observed for all other LNP formulations, particles at pH 4 were significantly smaller than those at pH 7.4 (Fig. 4I). Importantly, the use of GNPs show clearly that loaded LNP formulations can contain empty LNP, and that the fraction of empty LNP is dictated by the size of the payload (Fig. 4J). Thus, formulations entrapping larger nucleic acid sequences are more likely to contain empty LNP in the final formulation at pH 7.4.

Conclusions

The results presented in this work show that LNP systems, regardless of payload size, form through fusion of smaller particles as result of the pH neutralization step rather than the rapid-mixing step. This fusion process proceeds until the final particle accumulates sufficient PEG-lipid on the surface to inhibit further fusion. Thus, the LNP size is dictated by the PEG-lipid content, as expected larger proportions of PEG-lipids with smaller PEG moieties are required to achieve a given size. Finally, while the presence of payload does not affect subsequent fusion during pH neutralization, the size of the payload clearly influences the distribution of payload amongst the LNP formed. In particular, larger payloads such as mRNA, mcDNA and pDNA are more likely to lead to a population of loaded LNP and "empty" LNP.

In summary, the fusion-dependent process of LNP formation leads to a more detailed understanding of the mechanism of formation and the structures of LNP–nucleic acid com-

plexes formed. Such understanding is basic for the design of more potent LNP formulations of nucleic acid polymers for gene therapy applications.

Conflicts of interest

The authors have no conflicts to declare.

Acknowledgements

This work was supported by Foundation grant (FDN 148469) from the Canadian Institutes of Health Research, and a British Columbia Innovation Council Ignite grant. DW acknowledges the support by the Swiss National Science Foundation (SNF, Early Postdoc.Mobility Fellowship, Grant No. 174975). RvdM is supported by a VENI Fellowship (# 14385) from the Netherlands Organization for Scientific Research (NWO). HMGC is supported by the SNF Sinergia grant #180257 (to BT). The authors acknowledge N. Rimann for support with mcDNA production.

References

1 Press Release, I. Alnylam® Pharmaceuticals, http://investors.alnylam.com/news-releases/news-release-details/alnylam-announces-first-ever-fda-approval-rnai-therapeutic, accessed Aug. 11, 2018.
2 Press Release, I. Alnylam® Pharmaceuticals, http://investors.alnylam.com/news-releases/news-release-details/alnylam-announces-ema-acceptance-marketing-authorisation, accessed Feb. 1, 2018.
3 S. C. Semple, A. Akinc, J. Chen, A. P. Sandhu, B. L. Mui, C. K. Cho, D. W. Sah, D. Stebbing, E. J. Crosley, E. Yaworski, I. M. Hafez, J. R. Dorkin, J. Qin, K. Lam, K. G. Rajeev, K. F. Wong, L. B. Jeffs, L. Nechev, M. L. Eisenhardt, M. Jayaraman, M. Kazem, M. A. Maier, M. Srinivasulu, M. J. Weinstein, Q. Chen, R. Alvarez, S. A. Barros, S. De, S. K. Klimuk, T. Borland, V. Kosovrasti, W. L. Cantley, Y. K. Tam, M. Manoharan, M. A. Ciufolini, M. A. Tracy, A. de Fougerolles, I. MacLachlan, P. R. Cullis, T. D. Madden and M. J. Hope, *Nat. Biotechnol.*, 2010, **28**, 172–176.
4 M. Jayaraman, S. M. Ansell, B. L. Mui, Y. K. Tam, J. Chen, X. Du, D. Butler, L. Eltepu, S. Matsuda, J. K. Narayanannair, K. G. Rajeev, I. M. Hafez, A. Akinc, M. A. Maier, M. A. Tracy, P. R. Cullis, T. D. Madden, M. Manoharan and M. J. Hope, *Angew. Chem., Int. Ed.*, 2012, **51**, 8529–8533.
5 P. R. Cullis and M. J. Hope, *Mol. Ther.*, 2017, **25**(7), 1467–1475.
6 J. A. Kulkarni, P. R. Cullis and R. van der Meel, *Nucleic Acid Ther.*, 2018, **28**, 146–157.
7 L. B. Jeffs, L. R. Palmer, E. G. Ambegia, C. Giesbrecht, S. Ewanick and I. MacLachlan, *Pharm. Res.*, 2005, **22**, 362–372.
8 N. M. Belliveau, J. Huft, P. J. Lin, S. Chen, A. K. Leung, T. J. Leaver, A. W. Wild, J. B. Lee, R. J. Taylor, Y. K. Tam, C. L. Hansen and P. R. Cullis, *Mol. Ther.–Nucleic Acids*, 2012, **1**, e37.
9 J. A. Kulkarni, J. L. Myhre, S. Chen, Y. Y. C. Tam, A. Danescu, J. M. Richman and P. R. Cullis, *Nanomedicine*, 2016, **13**, 1377–1387.
10 A. K. Leung, Y. Y. Tam, S. Chen, I. M. Hafez and P. R. Cullis, *J. Phys. Chem. B*, 2015, **119**, 8698–8706.
11 J. A. Kulkarni, M. M. Darjuan, J. E. Mercer, S. Chen, R. van der Meel, J. L. Thewalt, Y. Y. C. Tam and P. R. Cullis, *ACS Nano*, 2018, **12**, 4787–4795.
12 A. K. Leung, I. M. Hafez, S. Baoukina, N. M. Belliveau, I. V. Zhigaltsev, E. Afshinmanesh, D. P. Tieleman, C. L. Hansen, M. J. Hope and P. R. Cullis, *J. Phys. Chem. C Nanomater. Interfaces*, 2012, **116**, 18440–18450.
13 M. J. W. Evers, J. A. Kulkarni, R. der Meel, P. R. Cullis, P. Vader and R. M. Schiffelers, *Small Methods*, 2018, **2**, 1700375.
14 A. Akinc, A. Zumbuehl, M. Goldberg, E. S. Leshchiner, V. Busini, N. Hossain, S. A. Bacallado, D. N. Nguyen, J. Fuller, R. Alvarez, A. Borodovsky, T. Borland, R. Constien, A. de Fougerolles, J. R. Dorkin, K. Narayanannair Jayaprakash, M. Jayaraman, M. John, V. Koteliansky, M. Manoharan, L. Nechev, J. Qin, T. Racie, D. Raitcheva, K. G. Rajeev, D. W. Sah, J. Soutschek, I. Toudjarska, H. P. Vornlocher, T. S. Zimmermann, R. Langer and D. G. Anderson, *Nat. Biotechnol.*, 2008, **26**, 561–569.
15 C. Waldner, M. Roose and G. U. Ryffel, *BMC Dev. Biol.*, 2009, **9**, 37.
16 H. M. Viecelli, R. P. Harbottle, S. P. Wong, A. Schlegel, M. K. Chuah, T. VandenDriessche, C. O. Harding and B. Thony, *Hepatology*, 2014, **60**, 1035–1043.
17 G. Basha, M. Ordobadi, W. R. Scott, A. Cottle, Y. Liu, H. Wang and P. R. Cullis, *Mol. Ther.–Nucleic Acids*, 2016, **5**, e363.
18 S. Hirota, C. T. de Ilarduya, L. G. Barron and F. C. Szoka Jr., *BioTechniques*, 1999, **27**, 286–290.
19 J. A. Kulkarni, Y. Y. C. Tam, S. Chen, Y. K. Tam, J. Zaifman, P. R. Cullis and S. Biswas, *Nanoscale*, 2017, **9**, 13600–13609.
20 S. Chen, Y. Y. Tam, P. J. Lin, A. K. Leung, Y. K. Tam and P. R. Cullis, *J. Controlled Release*, 2014, **196**, 106–112.
21 S. Chen, Y. Y. Tam, P. J. Lin, M. M. Sung, Y. K. Tam and P. R. Cullis, *J. Controlled Release*, 2016, **235**, 236–244.
22 P. Sengupta, D. Holowka and B. Baird, *Biophys. J.*, 2007, **92**, 3564–3574.
23 R. L. Thurmond, S. W. Dodd and M. F. Brown, *Biophys. J.*, 1991, **59**, 108–113.
24 N. Pardi, S. Tuyishime, H. Muramatsu, K. Kariko, B. L. Mui, Y. K. Tam, T. D. Madden, M. J. Hope and D. Weissman, *J. Controlled Release*, 2015, **217**, 345–351.
25 S. J. Eastman, C. Siegel, J. Tousignant, A. E. Smith, S. H. Cheng and R. K. Scheule, *Biochim. Biophys. Acta*, 1997, **1325**, 41–62.

26 M. Yanez Arteta, T. Kjellman, S. Bartesaghi, S. Wallin, X. Wu, A. J. Kvist, A. Dabkowska, N. Szekely, A. Radulescu, J. Bergenholtz and L. Lindfors, *Proc. Natl. Acad. Sci. U. S. A.*, 2018, **115**, E3351–E3360.

27 H. M. Grisch-Chan, A. Schlegel, T. Scherer, G. Allegri, R. Heidelberger, P. Tsikrika, M. Schmeer, M. Schleef, C. O. Harding, J. Haberle and B. Thony, *Mol. Ther.–Nucleic Acids*, 2017, **7**, 339–349.